Chemistry–A European Journal
Full Paper
doi.org/10.1002/chem.202000982
Chemistry Europe
European Chemical Societies Publishing

Photochemistry |Hot Paper|

Yield—not only Lifetime—of the Photoinduced Charge-Separated State in Iridium Complex–Polyoxometalate Dyads Impact Their Hydrogen Evolution Reactivity

Yusen Luo,[a, b] Salam Maloul,[c] Stefanie Schönweiz,[c] Maria Wächtler,[a, b] Carsten Streb,[c] and Benjamin Dietzek*[a, b, d]

Abstract: Covalently linked photosensitizer–polyoxometalate (PS-POM) dyads are promising molecular systems for light-induced energy conversion processes, such as "solar" hydrogen generation. To date, very little is known of their fundamental photophysical properties which affect the catalytic reactivity and stability of the systems. PS-POM dyads often feature short-lived photoinduced charge-separated states, and the lifetimes of these states are considered crucial for the function of PS-POM dyads in molecular photocatalysis. Hence, strategies have been developed to extend the lifetimes of the photoinduced charge-separated states, either by tuning the PS photophysics or by tuning the POM redox properties. Recently, some of us reported PS-POM dyads based on cyclometalated Ir^{III} complexes covalently linked to Anderson-type polyoxometalate. Distinct hydrogen evolution reactivity (HER) of the dyads was observed, which was tuned by varying the central metal ion *M* of the POM_M (*M* = Mn^{3+}, Co^{3+}, Fe^{3+}). In this manuscript, the photoinduced electron-transfer processes in the three Ir-POM_M dyads are investigated to rationalize the underlying reasons for the differences in HER activity observed. We report that upon excitation of the Ir^{III} complex, ultrafast (sub-ps) charge separation occurs, leading to different amounts of the charge-separated states ($Ir^{\bullet+}$-$POM_M^{\bullet-}$) generated in the different dyads. However, in all dyads studied, the resulting $Ir^{\bullet+}$-$POM_M^{\bullet-}$ species are short-lived (sub-ns) when compared to reference electron acceptors (e.g. porphyrins or fullerenes) reported in the literature. The reductive quenching of $Ir^{\bullet+}$-$POM_M^{\bullet-}$ by a sacrificial donor, triethyl amine (1 M), to generate the intermediate Ir-$POM_M^{\bullet-}$ is estimated to be very efficient (70–80 %) for all dyads studied. Based on this analyses, we conclude that the yield instead of the lifetime of the $Ir^{\bullet+}$-$POM_M^{\bullet-}$ charge-separated state determines the catalytic capacity of the dyads investigated. This new feature in the PS-POM photophysics could lead to new design criteria for the development of novel PS-POM dyads.

Introduction

Converting sunlight into chemical fuels is a key goal for green and sustainable energy technologies.[1] The generation of "solar hydrogen" requires the combination of several fundamental steps such as light-harvesting, charge-separation, charge-accumulation and catalysis (i.e. reduction of protons to H_2).[2] One strategy in artificial photosynthesis is to integrate all these fundamental processes into one supramolecular assembly, which at least contains a photoactive donor unit combined with an acceptor as catalytic unit for reduction reactions, respectively.[2] As a result of this molecular design, photoexcitation of the supramolecular assembly leads to the formation of a charge-separated state (CSS), in which the photoactive donor is oxidized, while the catalytic center is reduced. Ideally, the CSS is long lived and can thus react in a collision-induced reaction with a sacrificial electron donor or other reactants to give the desired product.[2] To-date a number of typically organic electron acceptors such as porphyrin or fullerene have been combined in this fashion with photoactive transition metal

[a] Dr. Y. Luo, Dr. M. Wächtler, Prof. Dr. B. Dietzek
Institute of Physical Chemistry and Abbe Center of Photonics
Friedrich-Schiller-University Jena, Helmholtzweg 4, 07743 Jena (Germany)
E-mail: benjamin.dietzek@uni-jena.de

[b] Dr. Y. Luo, Dr. M. Wächtler, Prof. Dr. B. Dietzek
Department Functional Interfaces
Leibniz Institute of Photonic Technology (IPHT), Albert-Einstein-Strasse 9
07745 Jena (Germany)
E-mail: benjamin.dietzek@leibniz-ipht.de

[c] S. Maloul, Dr. S. Schönweiz, Prof. Dr. C. Streb
Institute of Inorganic Chemistry I, Ulm University
Albert-Einstein-Allee 11, 89081 Ulm (Germany)

[d] Prof. Dr. B. Dietzek
Center for Energy and Environmental Chemistry Jena (CEEC Jena)
Friedrich-Schiller-University Jena, Philosophenweg 7a
07743 Jena (Germany)

Supporting information and the ORCID identification number(s) for the author(s) of this article can be found under: https://doi.org/10.1002/chem.202000982.

complex photosensitizers as donors.[2c,3] More recently, molecular metal oxides, or polyoxometalates (POMs), have emerged as inorganic electron acceptors in the field of artificial photosynthesis.[4] The beneficial properties of POMs as electron acceptors arise from their strong electron acceptor properties, multi-electron redox capabilities and catalytic activity in their reduced states.[4] The functionalization of POMs with visible light absorbing PS is critical, as POMs themselves typically only absorb light in the UV region. Thus, the design of covalently linked PS-POM dyads has recently emerged as a new design concept in POMs energy conversion.[5]

However, due to the synthetic challenges involved,[5j,k] currently there are only a few pioneering studies available. In these initial studies, Re^{I}, Ru^{II} and Ir^{III} complexes, porphyrins as well as BODIPY dyes have been used as photosensitizers, leading to possible applications in light-driven hydrogen evolution and photoelectrochemistry photovoltaics.[5] In these studies, the main focus was on Keggin-, Dawson- and Anderson-derivatives as their covalent functionalization is well-established.[5] However, in the reported PS-POM dyads either no charge-separated states, that is, $PS^{\bullet+}$-$POM^{\bullet-}$, or only relatively short-lived $PS^{\bullet+}$-$POM^{\bullet-}$ were detected upon excitation of the photosensitizers.[4,5a,b,d,e] The lifetimes of $PS^{\bullet+}$-$POM^{\bullet-}$ range from a few ps to the longest value reported up to now, which is about 500 ns.[5c,g,h] However, the lifetime of the photoinduced primary CSS, that is, $PS^{\bullet+}$-$POM^{\bullet-}$, is generally considered key to the function of PS-POM dyads in an artificial photosynthetic Scheme, as a long-lived CSS allows for reductive quenching of the oxidized PS by a sacrificial donor and subsequent light-driven or—depending on the specific reaction mechanism—dark processes. As POM-based dyads do not excel in terms of long lifetime of the CSS, this might become one of the limiting factors for developing POM-based artificial systems for solar fuels generation via multi-electron processes. Compared to the more frequently utilized Keggin- and Dawson-POMs, photoinduced dynamics in Anderson-POMs based assemblies are scarcely investigated:[5l] Hasenknopf and co-workers reported the linkage of Zn^{II} porphyrins to Dawson- and Anderson-POM and observed that photoinduced electron transfer takes place from the excited Zn^{II} porphyrin to the Dawson- but not to the Anderson-POM.[5l]

Some of us recently reported three PS-POM dyads based on Anderson-POM as electron acceptors, which were covalently linked to two cyclometalated Ir^{III} complexes as photosensitizer and electron donor ($(n\mathrm{Bu_4N})[M\mathrm{Mo_6O_{18}}\{(\mathrm{OCH_2})_3\mathrm{CNCH}(\mathrm{IrC_{33}H_{26}N_4})\}_2]$ molecular structure see the inset in Figure 1).[6] In these dyads, the central metal ion *M* of the POM_M was varied from $M = Mn^{3+}$ to Co^{3+} to Fe^{3+}.[6b] It was found that all Ir-POM_M dyads displayed hydrogen evolution reactivity (HER) in the presence of triethyl amine as a sacrificial electron donor and acetic acid as the proton source.[6b] The HER activity decreased from **Ir-POM_{Mn}** (TON = 80, measured over seven days) to **Ir-POM_{Co}** (TON = 34) to **Ir-POM_{Fe}** (TON = 20).[6b] Electrochemical data and DFT calculations indicated that the central *M* alters the redox properties of POM_M.[6b] For $M = Mn^{3+}$ the LUMO energy was the lowest.[6b] The modulation of the LUMO energy (3.95, 4.58 and 4.74 eV for POM_{Mn}, POM_{Co} and POM_{Fe}, respectively)[6b] in turn leads to a variation of the driving force for electron transfer, and hence, distinct rate constants for charge separation (which would significantly affect the yield of $Ir^{\bullet+}$-$POM_M^{\bullet-}$) and charge recombination (the stability of $Ir^{\bullet+}$-$POM_M^{\bullet-}$) are expected.

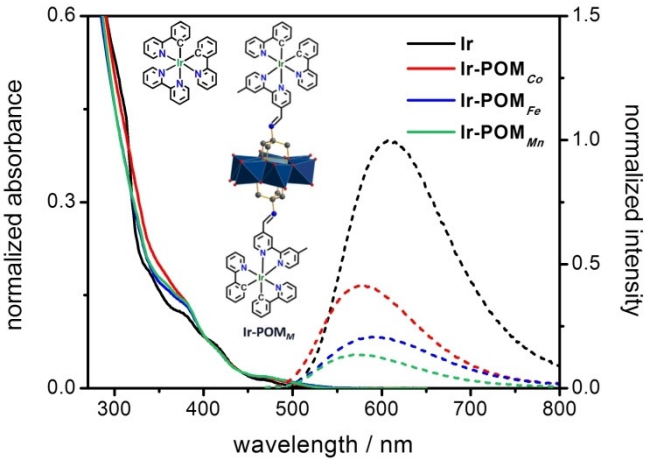

Figure 1. Normalized UV/Vis absorption spectra (isoabsorbing at 400 nm, $OD_{400\ nm} = 0.08$) and normalized emission spectra (dashed line, divided by the emission maximum of **Ir**, that is, $[Ir(bpy)(ppy)_2]PF_6$) in aerated DMF. The extinction coefficients for all compounds were reported in ref. [6b]. The metal oxo core of the Anderson-anion is $\{M\mathrm{Mo_6O_{24}}\}$ ($M = Co^{3+}$, Fe^{3+}, Mn^{3+}). Color code: MoO_6 octahedra, blue; metal cation *M*, cyan. POM and Ir^{III} complex are covalently connected via a -C=N- (imine) bond.

In this work, we explore the charge separation and charge recombination underlying the different HER activity of the aforementioned Ir-POM_M dyads. In order to do so, we performed femtosecond and nanosecond time-resolved spectroscopy and combine them with steady-state and time-resolved emission spectroscopy. The data presented indicates that the yield of the initial CSS is an important factor influencing the overall catalytic activity of Ir-POM_M. Thus, not only the lifetime of the CSS, $Ir^{\bullet+}$-$POM_M^{\bullet-}$, is to be considered as a photophysical metric to relate to the activity of such photocatalytically active dyads. Furthermore, on a more detailed notice, this work provides to the best of our knowledge the first example of a spectral characterization of a CSS in Anderson-POM based PS-POM dyads.

Results and Discussion

Steady-state emission spectra of Ir-POM_M dyads are depicted in Figure 1. The emission spectra of each compound were recorded at an optical density of 0.08 upon excitation at 400 nm. Compared to **Ir**, the emission intensity from the Ir^{III} unit is significantly decreased in **Ir-POM_{Mn}** and **Ir-POM_{Fe}** (by 86 and 79%, respectively). For **Ir-POM_{Co}** the emission intensity is only reduced by 58%. The partially quenched emission indicates that combining the Ir^{III} complex with the POM_M provides additional non-radiative decay channels for the excited Ir-POM_M dyads.

Photoinduced dynamics

The non-radiative decay pathways within the Ir-POM$_M$ dyads were studied by fs transient absorption (TA) spectroscopy. Figure 2 shows the fs TA spectra of **Ir**, **Ir-POM$_{Co}$** and **Ir-POM$_{Mn}$** obtained in aerated DMF upon excitation at 400 nm. The data recorded for **Ir-POM$_{Fe}$** are depicted in the ESI (Figure S1) as all dyads show very similar spectral features but different kinetics. The fs TA spectra of **Ir** upon excitation of the singlet metal-to-ligand charge transfer (MLCT) states resemble the spectral-temporal evolution as previously reported in literature:[7] A broad excited-state absorption (ESA) spanning from 350 to 750 nm corresponds to the absorption of ^{3}MLCT states in the photosensitizer and is observed immediately upon photoexcitation.[7b,c] Subsequently, two bands at 375 and at around 500 nm increase on a sub-10 ps timescale (Figure 2a, b). Based on spectro-electrochemical data, the ESA band at 375 nm (the orange dashed line in Figure 2c, for more information see Figure S2b) is assigned to the absorption of the reduced bpy ligand.[7b,c,8] Its increase at early times is attributed to interligand electron transfer (ILET) from an upper-lying ^{3}MLCT$_{ppy}$ state to the lower-lying ^{3}MLCT$_{bpy}$ state, a processes which has been established in literature.[7a,b]

Ir-POM$_{Co}$ and **Ir-POM$_{Mn}$** initially (i.e. at 0.4 ps after photoexcitation) display similar transient absorption features as **Ir**, that is, a rather broad but red-shifted ESA band in the visible region (Figure 2d, g). However, between 0.4 and 10 ps the dyads reveal spectral changes different to **Ir**: For one, the evolution of the ESA band in the visible region is faster in the dyads than in **Ir**. At 1.0 ps the band sharpens compared to **Ir**, that is, the FWHM (full width at half maximum) of the spectrum is reduced by 5, 16 and 11% compared to the data at 0.4 ps for **Ir**, **Ir-POM$_{Co}$** and **Ir-POM$_{Mn}$**, respectively. Meanwhile the spectral intensity already reaches a maximum (Figure 2d, g). Additionally, the ESA band in the UV region decreases instead of increasing as observed for **Ir** (Figure 2a, d and g). This is seen directly from the kinetic trace at 375 nm (blue lines in Figures 2b, e, h), which reflects the formation of a charge-separated state, that is, Ir$^{\bullet+}$-POM$_M^{\bullet-}$. The one-electron-reduced POM$_M$ (i.e. POM$_M^{\bullet-}$) has a negative absorption below 400 nm (Figure S3a, c, e), which apparently compensates the positive absorption signal of bpy$^{\bullet-}$ (Figure 2c, orange dashed line). At delay times longer than 100 ps, a pronounced decay of the overall TA signal is observed (Figure 2e, h) for both **Ir-POM$_{Co}$** and **Ir-POM$_{Mn}$**. However, within the experimentally accessible delay time range of 1.8 ns the decay is not complete, that is, a long-lived component is apparent in the fs data.

The quantitative interpretation of the fs TA data is based on a global fit.[9] For all compounds, two decay components and an offset are sufficient to describe the experimental data. The

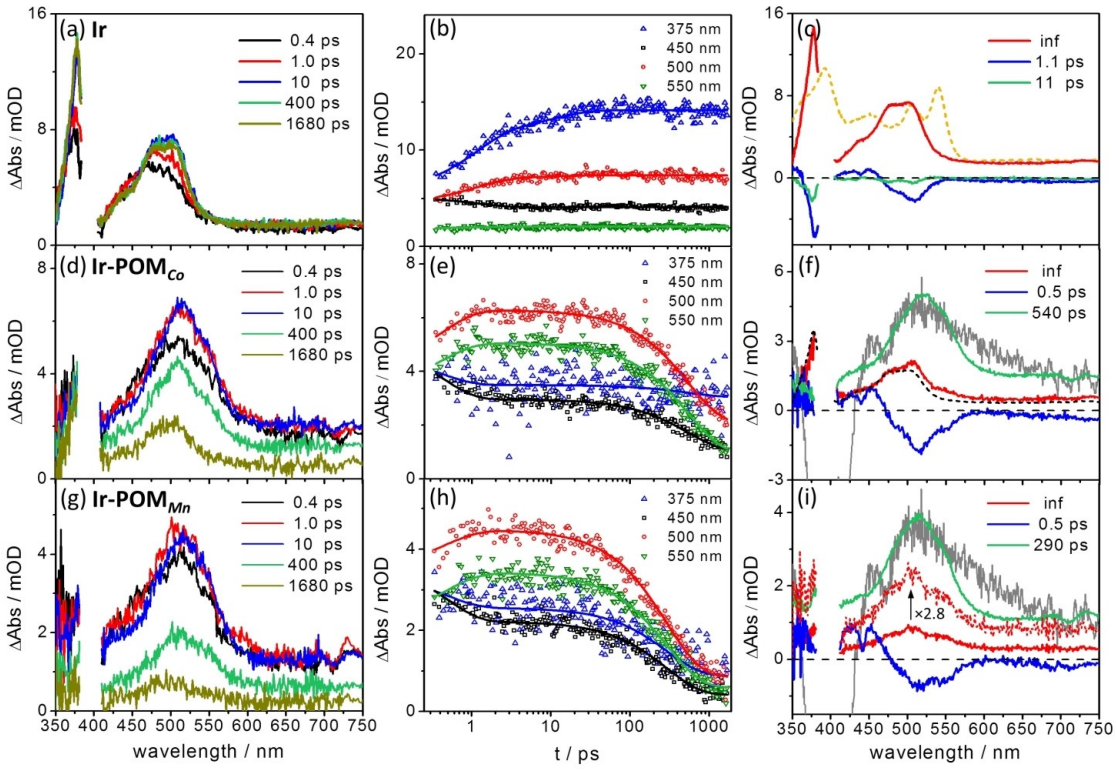

Figure 2. fs transient absorption spectra at selected delay times (left), selected kinetic traces with corresponding fit (middle) and decay-associated spectra (DAS) resulted from the global fit of the fs TA data (right) obtained upon excitation at 400 nm in aerated DMF for (a–c) **Ir**, (d–f) **Ir-POM$_{Co}$** and (g–i) **Ir-POM$_{Mn}$**. The orange dashed line in (c) is the spectroelectrochemical UV/Vis absorption difference spectrum of the reduced bpy ligand. The black dashed line in (f) is the infinite component in **Ir**. The grey line shows the simulated absorption spectrum of Ir$^{\bullet+}$-POM$_{Co}^{\bullet-}$ and Ir$^{\bullet+}$-POM$_{Mn}^{\bullet-}$ according to the spectroelectrochemical results (Figures S2 and S3). These spectra were arbitrarily scaled to integrate into the Figure. In (i) an enlarged amplitude (by a factor of 2.8) of the infinite component is shown for comparison.

decay-associated spectra (DAS, see ESI for a description on the DAS) and the corresponding characteristic time constants are given in Figure 2c, f, i. The kinetic components obtained for **Ir** are in agreement with previous work by Lochbrunner on the same complex:[7b,c] Following Lochbrunner's work, we assign the component associated with $\tau_1 = 1.1$ ps (Figure 2c) to vibrational relaxation within the ^{3}MLCT manifolds involving both ppy and bpy ligands. This is followed by ILET from a $^3MLCT_{ppy}$ to a $^3MLCT_{bpy}$ state. This process is characterized by $\tau_2 = 11$ ps. The long-lived species represents the long-lived thermalized $^3MLCT_{bpy}$ state, the decay of which to the electronic ground state is beyond the experimentally accessible delay-time range.

Considering the DAS-analysis of the fs TA data of the dyads, the fastest kinetic component is associated with a characteristic decay time $\tau_1 = 0.5$ ps. The corresponding spectral changes resemble the spectral shape of τ_1 in **Ir**, nonetheless comprising a slight red-shift compared to the spectra of the photosensitizer only (Figure 2f, i and Figure S1c; Figure S5a, c, e). Furthermore, DAS(τ_1) reveals a broader negative feature compared to the DAS(τ_1) in **Ir**. Specifically, in the dyads an increase of the transient absorption at 550 nm is associated with the τ_1-component (Figure 2f, i), which is not present in **Ir**. This ESA increase is due to the absorption of the reduced form of POM_M (i.e. $POM_M^{\bullet-}$, Figure S4) combined with possible contributions from the oxidized Ir^{III} center (i.e. $Ir^{\bullet+}$, Figure S2a. Note that the Ir photosensitizer in the dyads has additional substituents on the bpy ligand compared to reference **Ir** which might cause slight spectral difference to the MLCT and charge-separated states). This indicates that in Ir-POM_M electron transfer from the photo-excited Ir^{III} complex to the POM_M occurs rapid and in concert with vibrational relaxation of ^{3}MLCT states. The fast formation of $Ir^{\bullet+}$-$POM_M^{\bullet-}$, which indicates effective electronic coupling between the initially excited MLCT state of the photosensitizer and the POM_M, is corroborated by the difference spectrum of the DAS(τ_1) in **Ir** and Ir-POM_M (see Figure S5). Notably, the intensities of the TA signal at 550 nm in DAS (τ_1), which accounts for the charge-separation process, vary within the set of dyads (see Figure 3). Namely, ΔAbs at 550 nm in **Ir-POM$_{Mn}$** is roughly 2 times as high as that in **Ir-POM$_{Co}$** (Figure 3). This indicates different yields of $Ir^{\bullet+}$-$POM_M^{\bullet-}$ being generated in the dyads, that is, the yield of $Ir^{\bullet+}$-$POM_{Mn}^{\bullet-}$ is (two times) higher than that of $Ir^{\bullet+}$-$POM_{Co}^{\bullet-}$.

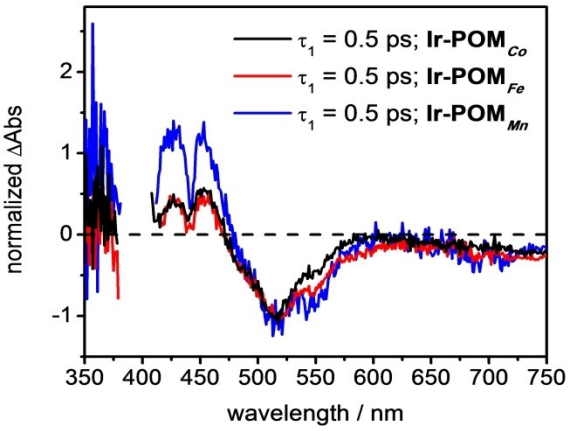

Figure 3. Comparison of the normalized (at 517 nm) decay-associated spectrum (DAS, associated with τ_1) in Ir-POM_M.

The 11-ps-component related to ILET in **Ir** is absent in the dyads. Instead, a hundreds of ps component is apparent, that is, $\tau_2 = 540$ and 290 ps for **Ir-POM$_{Co}$** and **Ir-POM$_{Mn}$**, respectively. This component reflects the decay of the charge-separated state $Ir^{\bullet+}$-$POM_M^{\bullet-}$, whose absorption has been simulated based on UV/Vis spectroelectrochemical data (Figure 2f, i, S2 and S3). In addition to τ_1 and τ_2, all dyads reveal a long-lived state, whose decay extends beyond the experimentally accessible delay-time window (~1.8 ns). The corresponding infinite component observed for **Ir-POM$_{Co}$** shows nearly identical features to that in **Ir** (Figure 2f), that is, a strong band below 400 nm and a moderate band (asymmetric and flat) in the visible region. This may indicate a decay of the $^3MLCT_{bpy}$ state in **Ir-POM$_{Co}$**. In contrast, the infinite component in **Ir-POM$_{Mn}$** (Figure 2i) and **Ir-POM$_{Fe}$** (Figure S1d) displays a rather distinct absorption at 550 nm. This points to a different long-lived state in **Ir-POM$_{Mn}$** and **Ir-POM$_{Fe}$** compared to **Ir-POM$_{Co}$**.

The nature of the long-lived state was assessed by ns TA spectroscopy (Figure 4). The ns TA spectra match the features of the infinite component in fs TA data. For **Ir-POM$_{Co}$**, similar to **Ir** (Figure S6), the ns TA signal decays mono-exponentially with a characteristic time constant of 120 ns (Figure 4c, d). For **Ir-POM$_{Mn}$** and **Ir-POM$_{Fe}$**, the shoulder at 550 nm disappears after 30 ns as revealed by the ns data in Figures 4b and S10a, while the overall decay of the differential absorption is slower. A global fit of the ns TA data yields a comparably short-lived component, $\tau_{ns1} = 30$ ns, and a relatively long-lived one, $\tau_{ns2} = 120$ ns (Figure S10b and S12b). The 120 ns-component in Ir-POM_M resembles the key spectral features of the 100 ns-component in **Ir** (Figure 4c and S14). Furthermore, the changes of its spectra and lifetime upon changing the solvent polarity (Figures S16–S20) correlate with the corresponding changes observed for **Ir**. Thus, we assign the 120 ns-component to the decay of the $^3MLCT_{bpy}$ state. The significant increase of τ_{ns2} upon exclusion of oxygen from the solution (120 vs. 640 ns in aerated and deaerated DMF, see Figure 4d, Figures S9, S11, S13 and S15) corroborate this assignment.[10]

Considering the 30 ns component, the ns TA results in DMF and DMSO indicate that it is a bright state whose lifetime is independent of solvent polarity ($\tau_{ns1} = 30$ ns in DMF and $\tau_{ns1} = 40$ ns in DMSO, Figures S10d, S12d, S18d and S19d). These properties exclude the possibility of a CSS being formed. On the contrary, τ_{ns1} doubles upon exclusion of oxygen from DMF (inset in Figure 4d; Figure S11d and S13d). Furthermore, its energetic position appears to be drastically shifted when changing the solvent from DMF (emission at 550 nm) to DMSO (emission at 680 nm). Nevertheless, the nature of the 30 ns component is beyond the scope of this study because the different HER activity of Ir-POM_M is not impacted by the presence of this state: Both dyads, which reveal this component, **Ir-POM$_{Mn}$** and **Ir-POM$_{Fe}$** display rather different HER activity (TON = 80 vs. 20, respectively).[6b] **Ir-POM$_{Co}$**, whose ns-decay does not reveal the 30-ns component, displays an intermediate TON of 34, which is 70% higher than that of **Ir-POM$_{Fe}$**.[6b]

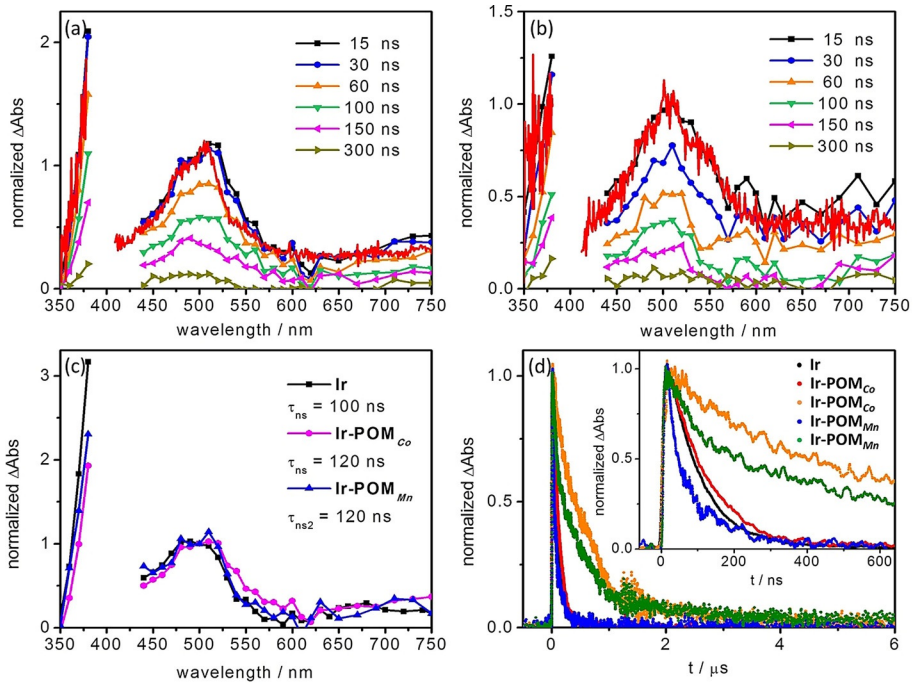

Figure 4. ns transient absorption spectra of (a) **Ir-POM$_{Co}$** and (b) **Ir-POM$_{Mn}$** collected upon excitation at 410 nm in aerated DMF. The spectrum of the infinite component in fs TA data (red line) is added for comparison. The fs TA spectrum and ns TA spectrum (at 15 ns) were normalized at 510 nm. (c) Normalized (at 500 nm) global fit results of the ns TA data of **Ir**, **Ir-POM$_{Co}$** and **Ir-POM$_{Mn}$**. Only the long-lived species in **Ir-POM$_{Mn}$** is incorporated. (d) Normalized integrated kinetic traces (between 450 and 750 nm of the ns TA spectra) in aerated (black, red and blue for **Ir**, **Ir-POM$_{Co}$** and **Ir-POM$_{Mn}$**, respectively) and deaerated DMF (yellow and green for **Ir-POM$_{Co}$** and **Ir-POM$_{Mn}$**, respectively). Inset: The enlargement of the time region up to 640 ns.

Relaxation model

Scheme 1 summarizes the photophysical picture of Ir-POM$_M$ as it emerges from the time-resolved spectroscopy. According to the fs TA results, photoinduced electron transfer in the dyads occurs concertedly with vibrational energy dissipation, indicating that electron transfer is most efficient from vibrationally hot ^{3}MLCT states (Scheme 1). Considering electron transfer from the individual ^{3}MLCT states intrinsic to the system, the driving force for electron transfer can be estimated by the Rehm–Weller equation $\Delta G_{CS} = e(E_{D+/D} - E_{A/A-}) - E_{00} - (e^2 / 4\pi\varepsilon_0\varepsilon R_{DA})$.[11] As the ^{3}MLCT$_{ppy}$ state is energetically higher than the ^{3}MLCT$_{bpy}$ state (i.e. a larger E_{00}),[7] a more negative driving force will be induced. Hence, we cannot exclude the direct through-space electron transfer from the hot ^{3}MLCT$_{ppy}$ to the POM (Scheme 1). The presence of this direct electron-transfer pathway explains the absence of ILET in the dyads Ir-POM$_M$ as compared to **Ir**, where ILET dominates the 11-ps process. Besides, ultrafast electron transfer from the initially excited hot ^{1}MLCT states (see resonance Raman data in Figure S21), which would have more favorable driving forces, might be operative as well. However, due to the temporal resolution (~110 fs) of the fs TA setup such ultrafast process cannot be explored.

τ_2 in the dyads is attributed to charge recombination yielding the decay of Ir$^{\bullet+}$-POM$_M^{\bullet-}$. The lifetime of Ir$^{\bullet+}$-POM$_M^{\bullet-}$ depends on the central metal ion *M*, that is, Ir$^{\bullet+}$-POM$_{Mn}^{\bullet-}$ (290 ps) < Ir$^{\bullet+}$-POM$_{Fe}^{\bullet-}$ (430 ps) < Ir$^{\bullet+}$-POM$_{Co}^{\bullet-}$ (540 ps). In hydrogen evolution experiment investigating the Ir-POM$_M$ dyads studied here, the concentration of the sacrificial donor (1 M) was 10000 higher than that of the dyads (0.1 mM).[6b] Under these conditions, the diffusion-limited rate constant of the sacrificial donor for quenching is about 7.6×10^9 s^{-1} (calculated by multiplying the diffusion-limited rate constant in DMF, 7.6×10^9 M^{-1}s^{-1}, with the concentration of sacrificial donor, 1 M). This rate corresponds to a characteristic time constant of 126 ps.[14,15] This indicates that the characteristic lifetimes of the Ir$^{\bullet+}$-POM$_M^{\bullet-}$ (τ_2 = 290–540 ps) provides a sufficiently large temporal window for the interaction with the sacrificial donor, yielding Ir-POM$_M^{\bullet-}$ as an essential intermediate in the photocatalytic cycle. Based on the time constants for diffusion and charge recombination (τ_2), the quenching efficiency by the sacrificial donor is estimated to be 70 and 80% in **Ir-POM$_{Mn}$** and **Ir-POM$_{Co}$**, respectively. However, the HER activity of **Ir-POM$_{Mn}$** (TON = 80) was reported to be 2.4 times as high as that of **Ir-POM$_{Co}$** (TON = 34).[6b] Therefore, we conclude that the HER activity of the dyads as observed under conventionally employed experimental conditions[6b] seems not governed by the lifetimes of the charge-separated state Ir$^{\bullet+}$-POM$_M^{\bullet-}$. Instead, this study suggests that the yield of Ir$^{\bullet+}$-POM$_M^{\bullet-}$ plays an important role in the catalytic capacity of Ir-POM$_M$. As discussed above, the yield of Ir$^{\bullet+}$-POM$_{Mn}^{\bullet-}$ is roughly twice the yield of Ir$^{\bullet+}$-POM$_{Co}^{\bullet-}$. This finding is consistent with the ratio of the HER activity of the respective dyads. Furthermore, from the perspective of photostability, more efficient hot ^{3}MLCT→POM electron transfer results in a reduced population of the long-lived thermalized ^{3}MLCT state. Thereby, ^{3}MLCT→POM electron transfer reduces the potential for destructive side-reactions taking place from the high-energy ^{3}MLCT state, which might

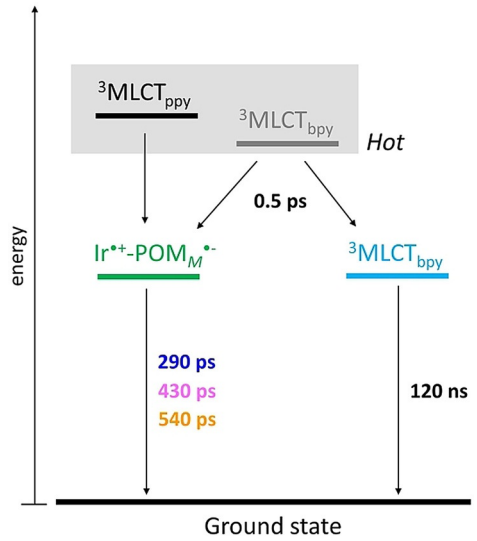

Scheme 1. Simplified energy-level diagrams of **Ir-POM$_{Co}$** (orange), **Ir-POM$_{Fe}$** (pink) and **Ir-POM$_{Mn}$** (blue). The color code indicates the corresponding time constants for each compound. The same time constants for dyads are shown in black. According to the electrochemical results, the energetic level of Ir$^{\bullet+}$-POM$_M$$^{\bullet-}$ is estimated to be 2.25 ~ 2.35 eV in DMF.[6] The energetic level of the thermalized ^{3}MLCT$_{bpy}$ state can be estimated from the steady-state emission spectrum of [Ir(ppy)$_2$(bpy)]$^+$. At 77 K, the emission maximum is at 532 nm (2.33 eV) for [Ir(ppy)$_2$(bpy)]$^+$ (^{3}MLCT$_{bpy}$ is the lowest state) in frozen 2-MeTHF.[12] Note: due to the temporal resolution (~110 fs) of the fs TA setup and our data-processing (a temporal window of 200 fs around time-zero was excluded to avoid contributions of coherent artifacts[13]) any ultrafast processes taking place within 200 fs, for example, intersystem crossing or possible ^{1}MLCT→POM electron transfer, cannot be probed. Hence, the photophysical model derived from the data presented in this manuscript focuses on the decay of the ^{3}MLCT states.

lead to decomposition of the Ir-POM$_M$ dyad under catalytic conditions. Hence, an increased yield of the CSS might benefit the catalytic HER activity twofold by increasing the yield of a critical charge-transfer intermediate of the catalytic cycle and by diminishing the potential for detrimental side reactions. Our work points out that for a good performance of the catalysts the photoinduced CSS should be sufficiently long-lived for the subsequent reactions (i.e. to react with external reactants according to the specific reaction schemes). When the decay dynamics of the CSS itself are comparable to the rates of subsequent reactions, extending the lifetimes of the CSS would not improve the function of the catalysts. At this point, the yields of CSS have to be considered. In this respect, proper molecular design for fast charge separation (e.g. by inducing a larger driving force or a stronger electronic coupling), which can compete with the decay of the excited state itself (e.g. the cooling process in Scheme 1), could promote the yields of CSS.

Conclusions

The photoinduced electron transfer dynamics underlying the distinct catalytic capacity (**Ir-POM$_{Mn}$** > **Ir-POM$_{Co}$** > **Ir-POM$_{Fe}$**) of three covalently linked Ir-POM$_M$ dyads were investigated spectroscopically. The central metal ion *M* of POM$_M$, that is, [*M*Mo$_6$O$_{24}$]$^{n-}$, was changed from Mn^{3+} to Co^{3+} to Fe^{3+} to modify the redox properties of the POM$_M$ acceptors.[6b] As a consequence of this modification, different photophysical properties of the Ir-POM$_M$ dyads can be expected. Irrespective of the central metal ion *M*, however, ultrafast charge separation was observed, which takes place concertedly with vibrational energy dissipation. The yields and the lifetimes of the charge-separated state, that is, Ir$^{\bullet+}$-POM$_M$$^{\bullet-}$, vary with the nature of the POM$_M$. The yields of Ir$^{\bullet+}$-POM$_M$$^{\bullet-}$ decrease in the order **Ir-POM$_{Mn}$** > **Ir-POM$_{Fe}$** > **Ir-POM$_{Co}$**. The lifetimes of the CSS show the inverse, that is, Ir$^{\bullet+}$-POM$_{Mn}$$^{\bullet-}$ (290 ps) < Ir$^{\bullet+}$-POM$_{Fe}$$^{\bullet-}$ (430 ps) < Ir$^{\bullet+}$-POM$_{Co}$$^{\bullet-}$ (540 ps). Considering the diffusion-limited rate constant for intermolecular quenching process with the lifetimes of Ir$^{\bullet+}$-POM$_M$$^{\bullet-}$, the sub-ns lifetime is sufficient to allow for efficient capture of the Ir$^{\bullet+}$-POM$_M$$^{\bullet-}$ by collision with a sacrificial donor under catalytic conditions (70–80%). We thus conclude that the yield of Ir$^{\bullet+}$-POM$_M$$^{\bullet-}$ plays an important role in affecting the catalytic capacity of Ir-POM$_M$ under the given kinetic conditions. Thus, considering the yield of the formation of the charge-separated states presents and additional photophysical metric—next to the conventionally considered lifetime of charge separation—to target in order to device catalytically efficient PS-POM dyads. To improve the yields of the photoinduced charge-separated states in the Ir-POM$_M$ system, it might be useful to increase either the driving force or the electronic coupling between the Ir^{III} complex and the POM$_M$ to accelerate the charge-separation process. For this purpose, decreasing the distance between PS and POM$_M$, or using a different POM which is easier to be reduced would be promising choices.

Experimental Section

General

Steady-state UV/Vis absorption spectra were recorded in a quartz cell with 1 mm path length (for fs transient absorption experiment, JASCO V-670 spectrophotometer) and with 1 cm path length (for ns transient absorption experiment, Cary 5000 UV/Vis spectrometer, Varian, USA). For all time-resolved experiments, the stability of samples was ensured by recording the steady-state UV/Vis absorption spectra before and after every measurement. The steady-state emission spectra were recorded in a quartz cell with 1 cm path length on a FLS980 spectrofluorimeter (Edinburgh).

Electrochemistry and spectroelectrochemistry

Cyclic voltammetry (CV) and spectroelectrochemistry (SEC) measurements were performed in a home-built three-electrode thin-layer cell with a path length of 1 mm. The three-electrode system consists of a glassy carbon working electrode, a platinum wire counter electrode and an Ag/AgCl reference electrode. CV and potential-controlled monitoring were performed using a computer-controlled potentiostat (VersaSTAT 3, Princeton Applied Research). All potentials given in the manuscript refer to the ferrocene/ferrocenium couple as internal standard. The corresponding UV/Vis spectra were recorded on a single-beam spectrometer (Avantes, Avalight-DH-S-BAL) at room temperature.

Time-resolved spectroscopy

Femtosecond (fs) transient absorption spectra were collected by using a previously reported home-built pump-probe laser system which is based on an amplified Ti: Sapphire oscillator (Libra, Coherent Inc.).[16] All compounds were excited by pump pulse centered at 400 nm (TOPASwhite, Lightconversion Ltd.) with a duration of 110 fs. The power of the pump beam was kept at 0.4 mW and the beam diameter of the pump was 145 μm at the sample position. This corresponds to 0.95×10^{20} photons m^{-2} per pulse. A white light supercontinuum generated by focusing a fraction of the fundamental in a rotating CaF_2 plate is used to probe the samples in a wide spectral range (340 to 750 nm). The probe beam is delayed in time with respect to the pump beam by means of an optical delay line and the polarization between probe and pump is set at the magic angle (54.7°). Each solution (optical density ca. 0.2 at the excitation wavelength) was kept in a 1 mm quartz cuvette. Transient absorption data were displayed after chirp correction. The transient absorption data was analyzed by a global multi-exponential fit after exclusion of a temporal window of 200 fs around time-zero in order to avoid contributions of the coherent-artifact region to the data analysis.[13] Furthermore, a spectral band of 20 nm around the pump-wavelength is omitted from the data analysis due to pump-scatter in this spectral range.

Nanosecond (ns) transient absorption spectra[16c] were collected to study the long-lived species in the fs transient absorption data. The pump pulses centered at 410 nm were produced by a Continuum OPO Plus which is pumped by an continuum surelite Nd:YAG laser system (pulse duration 5 ns, repetition rate 10 Hz). The probe light is provided by a 75 W xenon arc lamp. Spherical concave mirrors are used to focus the probe beam into the samples and then send the beam to the monochromator (Acton, Princeton Instruments) and detected by a photomultiplier tube (Hamamatsu R928). The signal is amplified and processed by a commercially available detection system (Pascher Instruments AB). For all measurements, the power of the pump beam was kept at 0.35 mJ. ns TA spectra were recorded by using a bandpass (325–385 nm) and a long pass filter (435 nm) to eliminate the pump scattering. Time-resolved emission spectra were collected with the use of a long pass filter (435 nm) as well. Each sample was freshly prepared and the optical density (ca. 0.3) at the excitation wavelengths 410 nm was kept the same. All measurements were performed in 1 cm path length fluorescence cuvettes. Oxygen-free solutions were obtained by at least five freeze-pump-thaw cycles.

Resonance Raman spectroscopy

Resonance Raman (RR) spectra were recorded through excitation by a 405 nm diode laser (TopMode-405-HP, Toptica, Germany) and detected by an IsoPlane 160 spectrometer (Princeton Instruments, USA) with an entrance slit width of 0.05 mm, a focal length of 750 mm, and grating 2400 grooves mm^{-1}. The excitation energy was attenuated to around 8 mW. The Raman signals were recorded by a thermoelectrically cooled PIXIS eXcelon camera (Princeton Instruments, USA). The Raman spectra were initially baseline corrected and normalized with respect to a solvent band, that is, to the signal at 1404 cm^{-1} for DMF.

Acknowledgements

This research is supported by the CataLight CRC/TRR 234 (project number 364549901, projects A1 and A4 and Z2) funded by the Deutsche Forschungsgemeinschaft (DFG). S.M. thanks the Deutscher Akademischer Austauschdienst DAAD for a Ph.D. fellowship.

Conflict of interest

The authors declare no conflict of interest.

Keywords: catalytic mechanisms · hydrogen evolution · photochemistry · photophysics · polyoxometalates

[1] a) D. G. Nocera, *Acc. Chem. Res.* **2017**, *50*, 616–619; b) K. E. Dalle, J. Warnan, J. J. Leung, B. Reuillard, I. S. Karmel, E. Reisner, *Chem. Rev.* **2019**, *119*, 2752–2875.

[2] a) S. Fukuzumi, K. Ohkubo, T. Suenobu, *Acc. Chem. Res.* **2014**, *47*, 1455–1464; b) M. Gilbert, B. Albinsson, *Chem. Soc. Rev.* **2015**, *44*, 845–862; c) M. Rudolf, S. V. Kirner, D. M. Guldi, *Chem. Soc. Rev.* **2016**, *45*, 612–630; d) N. T. La Porte, J. F. Martinez, S. Chaudhuri, S. Hedström, V. S. Batista, M. R. Wasielewski, *Coord. Chem. Rev.* **2018**, *361*, 98–119; e) B. Zhang, L. Sun, *Chem. Soc. Rev.* **2019**, *48*, 2216–2264; f) S. Neumann, C. Kerzig, O. S. Wenger, *Chem. Sci.* **2019**, *10*, 5624–5633.

[3] a) L. Flamigni, J.-P. Collin, J.-P. Sauvage, *Acc. Chem. Res.* **2008**, *41*, 857–871; b) O. S. Wenger, *Coord. Chem. Rev.* **2009**, *253*, 1439–1457; c) O. S. Wenger, *Coord. Chem. Rev.* **2015**, *282–283*, 150–158; d) K. Barthelmes, A. Winter, U. S. Schubert, *Dalton Trans.* **2016**, *45*, 14855–14882; e) Y. Luo, K. Barthelmes, M. Wächtler, A. Winter, U. S. Schubert, B. Dietzek, *Chem. Eur. J.* **2017**, *23*, 4917–4922; f) Y. Luo, K. Barthelmes, M. Wächtler, A. Winter, U. S. Schubert, B. Dietzek, *J. Phys. Chem. C* **2017**, *121*, 9220–9229.

[4] a) J. J. Walsh, A. M. Bond, R. J. Forster, T. E. Keyes, *Coord. Chem. Rev.* **2016**, *306*, 217–234; b) G. Izzet, F. Volatron, A. Proust, *Chem. Rec.* **2017**, *17*, 250–266; c) J. M. Cameron, D. J. Wales, G. N. Newton, *Dalton Trans.* **2018**, *47*, 5120–5136; d) L. Chen, W.-L. Chen, X.-L. Wang, Y.-G. Li, Z.-M. Su, E.-B. Wang, *Chem. Soc. Rev.* **2019**, *48*, 260–284; e) A. J. Kibler, G. N. Newton, *Polyhedron* **2018**, *154*, 1–20.

[5] a) K. J. Elliott, A. Harriman, L. Le Pleux, Y. Pellegrin, E. Blart, C. R. Mayer, F. Odobel, *Phys. Chem. Chem. Phys.* **2009**, *11*, 8767–8773; b) B. Matt, C. Coudret, C. Viala, D. Jouvenot, F. Loiseau, G. Izzet, A. Proust, *Inorg. Chem.* **2011**, *50*, 7761–7768; c) B. Matt, X. Xiang, A. L. Kaledin, N. Han, J. Moussa, H. Amouri, S. Alves, C. L. Hill, T. Lian, D. G. Musaev, G. Izzeta, A. Proust, *Chem. Sci.* **2013**, *4*, 1737–1745; d) F. A. Black, A. Jacquart, G. Toupalas, S. Alves, A. Proust, I. P. Clark, E. A. Gibson, G. Izzet, *Chem. Sci.* **2018**, *9*, 5578–5584; e) A. Yokoyama, T. Kojima, K. Ohkubo, M. Shiro, S. Fukuzumi, *J. Phys. Chem. A* **2011**, *115*, 986–997; f) C. Zhao, Z. Huang, W. Rodríguez-Córdoba, C. S. Kambara, K. P. O'Halloran, K. I. Hardcastle, D. G. Musaev, T. Lian, C. L. Hill, *J. Am. Chem. Soc.* **2011**, *133*, 20134–20137; g) Y. Luo, M. Wächtler, K. Barthelmes, A. Winter, U. S. Schubert, B. Dietzek, *Chem. Commun.* **2018**, *54*, 2970–2973; h) Y. Luo, M. Wächtler, K. Barthelmes, A. Winter, U. S. Schubert, B. Dietzek, *Phys. Chem. Chem. Phys.* **2018**, *20*, 11740–11748; i) C. Allain, D. Schaming, N. Karakostas, M. Erard, J.-P. Gisselbrecht, S. Sorgues, I. Lampre, L. Ruhlmann, B. Hasenknopf, *Dalton Trans.* **2013**, *42*, 2745–2754; j) A. Proust, B. Matt, R. Villanneau, G. Guillemot, P. Gouzerh, G. Izzet, *Chem. Soc. Rev.* **2012**, *41*, 7605–7622; k) E. Hampson, J. M. Cameron, S. Amin, J. Kyo, J. A. Watts, H. Oshio, G. N. Newton, *Angew. Chem. Int. Ed.* **2019**, *58*, 18281–18285; *Angew. Chem.* **2019**, *131*, 18449–18453.

[6] a) S. Schönweiz, S. A. Rommel, J. Kübel, M. Micheel, B. Dietzek, S. Rau, C. Streb, *Chem. Eur. J.* **2016**, *22*, 12002–12005; b) S. Schönweiz, M. Heiland, M. Anjass, T. Jacob, S. Rau, C. Streb, *Chem. Eur. J.* **2017**, *23*, 15370–15376.

[7] a) E. Pomarico, M. Silatani, F. Messina, O. Braem, A. Cannizzo, E. Barranoff, J. H. Klein, C. Lambert, M. Chergui, *J. Phys. Chem. C* **2016**, *120*, 16459–16469; b) S. Tschierlei, A. Neubauer, N. Rockstroh, M. Karnahl, P. Schwarzbach, H. Junge, M. Bellerd, S. Lochbrunner, *Phys. Chem. Chem. Phys.* **2016**, *18*, 10682–10687; c) R. Bevernaegie, L. Marcélis, A. Moreno-Betancourt, B. Laramée-Milette, G. S. Hanan, F. Loiseau, M. Sliwa, B. Elias, *Phys. Chem. Chem. Phys.* **2018**, *20*, 27256–27260.

[8] S. I. Bokarev, D. Hollmann, A. Pazidis, A. Neubauer, J. Radnik, O. Kühn, S. Lochbrunner, H. Junge, M. Beller, A. Brückner, *Phys. Chem. Chem. Phys.* **2014**, *16*, 4789 – 4796.
[9] a) R. Siebert, A. Winter, U. S. Schubert, B. Dietzek, J. Popp, *Phys. Chem. Chem. Phys.* **2011**, *13*, 1606 – 1617; b) C. Reichardt, T. Sainuddin, M. Wächtler, S. Monro, S. Kupfer, J. Guthmuller, S. Gräfe, S. McFarland, B. Dietzek, *J. Phys. Chem. A* **2016**, *120*, 6379 – 6388.
[10] a) K. Kawaoka, A. U. Khan, D. R. Kearns, *J. Chem. Phys.* **1967**, *46*, 1842 – 1853; b) A. A. Abdel-Shafi, D. R. Worrall, A. Y. Ershov, *Dalton Trans.* **2004**, 30 – 36.
[11] a) D. Rehm, A. Weller, *Isr. J. Chem.* **1970**, *8*, 259 – 271; b) E. Göransson, J. Boixel, J. Fortage, D. Jacquemin, H.-C. Becker, E. Blart, L. Hammarström, F. Odobel, *Inorg. Chem.* **2012**, *51*, 11500 – 11512.
[12] S. Ladouceur, D. Fortin, E. Zysman-Colman, *Inorg. Chem.* **2010**, *49*, 5625 – 5641.
[13] a) S. A. Kovalenko, A. L. Dobryakov, J. Ruthmann, N. P. Ernsting, *Phys. Rev. A* **1999**, *59*, 2369 – 2384; b) B. Dietzek, T. Pascher, V. Sundström, A. Yartsev, *Laser Phys. Lett.* **2007**, *4*, 38 – 43.
[14] Note: the calculated time constant for intermolecular quenching only considered the rate of encounter between the photo-excited dyad and the sacrificial donor. In reality this process would kinetically compete with backward electron transfer within the solvent cage to reform the original ground-state species. These processes together with the escape of the redox species out of the cage into bulk solution determine the yield of the Ir-$POM_M^{\bullet-}$ intermediate. But we do not expect that the intermolecular kinetics would depend drastically on the nature of the reduced state of Ir-POM_M.
[15] a) M. Georgopoulos, M. Z. Hoffman, *J. Phys. Chem.* **1991**, *95*, 7717 – 7721; b) K. A. Hötzer, A. Klingert, T. Klumpp, E. Krissinel, D. Bürssner, U. E. Steiner, *J. Phys. Chem. A* **2002**, *106*, 2207 – 2217.
[16] a) M. Karnahl, C. Kuhnt, F. Ma, A. Yartsev, M. Schmitt, B. Dietzek, S. Rau, J. Popp, *ChemPhysChem* **2011**, *12*, 2101 – 2109; b) J. Kübel, R. Schroot, M. Wächtler, U. S. Schubert, B. Dietzek, M. Jäger, *J. Phys. Chem. C* **2015**, *119*, 4742 – 4751; c) K. Barthelmes, J. Kübel, A. Winter, M. Wächtler, C. Friebe, B. Dietzek, U. S. Schubert, *Inorg. Chem.* **2015**, *54*, 3159 – 3171.

Manuscript received: February 24, 2020
Accepted manuscript online: April 1, 2020
Version of record online: May 29, 2020

